Article

Study of Radiation Embitterment and Degradation Processes of Li₂ZrO₃ Ceramic under Irradiation with Swift Heavy Ions

Baurzhan Abyshev [1], Artem L. Kozlovskiy [2,3,*] , Kassym Sh Zhumadilov [1] and Alex V. Trukhanov [4,5,6]

[1] Engineering Profile Laboratory, L.N. Gumilyov Eurasian National University, Nur-Sultan 010008, Kazakhstan; baurzhan_abyshev@gmail.com (B.A.); zhumadilov_ksh@enu.kz (K.S.Z.)

[2] Laboratory of Solid State Physics, The Institute of Nuclear Physics, Almaty 050032, Kazakhstan

[3] Institute of Geology and Oil and Gas Business, Satbayev University, Almaty 0500032, Kazakhstan

[4] Laboratory of Magnetic Films Physics, Scientific-Practical Materials Research Centre of National Academy of Sciences of Belarus, 220072 Minsk, Belarus; truhanov86@mail.ru

[5] Laboratory of Single Crystal Growth, South Ural State University, Lenin prospekt, Chelyabinsk 76, 454080 Chelyabinsk, Russia

[6] Department of Technology of Electronics Materials, National University of Science and Technology MISiS, Leninsky Prospekt 4, 119049 Moscow, Russia

* Correspondence: kozlovskiy.a@inp.kz; Tel./Fax: +7-7024413368

Abstract: The work is devoted to the study of radiation damage and subsequent swelling processes of the surface layer of Li₂ZrO₃ ceramics under irradiation with heavy Xe²²⁺ ions, depending on the accumulation of the radiation dose. The samples under study were obtained using a mechanochemical synthesis method. The samples were irradiated with heavy Xe²²⁺ ions with an energy of 230 MeV at irradiation fluences of 10^{11}–10^{16} ion/cm². The choice of ion types is due to the possibility of simulating the radiation damage accumulation processes as a result of the implantation of Xe²²⁺ ions and subsequent atomic displacements. It was found that, at irradiation doses above 5×10^{14} ion/cm², point defects accumulate, which leads to a disordering of the surface layer and a subsequent decrease in the strength and hardness of ceramics. At the same time, the main process influencing the decrease in resistance to radiation damage is the crystal structure swelling as a result of the accumulation of defects and disordering of the crystal lattice.

Keywords: radiation damage; heavy ions; blankets; lithium-containing ceramics; disordering

1. Introduction

As is known, the choice of blanket materials for the reproduction of tritium is one of the important criteria for the development of the nuclear industry and the creation of new nuclear installations [1,2]. At the same time, the use of blanket materials, not only for the reproduction of tritium, but also for obtaining energy, made it possible to develop a new direction of nuclear reactors called hybrid reactors. The scheme of such reactors is based on two mechanisms: the course of reactions of synthesis of hydrogen isotopes under the action of neutrons, followed by the accumulation of tritium and helium, as well as the course of nuclear reactions for the release of heat, accompanied by the formation of fission fragments. At the same time, for the accumulation of tritium for the purpose of its subsequent use, one of the proposed materials with a number of unique properties are solid oxide ceramics based on titanates, orthosilicates or lithium metazirconates [3–5]. The interest in these types of ceramics is due to the possibility of using them as breeders of tritium in order to further maintain nuclear reactions due to the burnout of lithium and the formation of tritium in a reaction of the ⁶Li + n → ⁴He + T + 4.0 MeV type [6].

One of the important issues in the field of using ceramic materials as blankets or structural materials for nuclear power is their operational safety, which includes data on resistance to radiation damage and the accumulation of radiation defects in the structure [7–10]. As is known, the long-term operation of nuclear fuel leads to the formation of a large

number of induced radiation defects, which are formed both as a result of transmutation reactions with neutrons and during the interaction of fragments of uranium fuel nuclei with the matrix material [11–15]. The result of such processes is the radiation damage accumulation, which, in turn, can adversely affect the physicochemical properties of ceramics, as well as their strength, hardness and resistance to embrittlement [16–18]. At the same time, it is known that, in spite of a high thermochemical stability and mass transfer characteristics, as well as a compatibility with other types of structural materials, lithium-containing ceramics based on lithium metazirconates have a high anisotropy in the coefficient of thermal expansion [19,20]. This, in turn, can lead to the formation of microcracks and destruction of the material as a result of long-term operation and the radiation damage accumulation.

It is also prudent to mention that, in addition to radiation damage caused by fission fragments arising in the structure of the surface layer of ceramics, a significant contribution to the change in the stability indices is made by damage caused by neutron irradiation [21], gamma radiation and electron radiation [22–24], as well as low-energy ions (with energies less than 500–1000 keV) [25,26]. Generally, interactions with gamma and electron radiation are accompanied by a change in the electron density in ceramics due to the large contribution of interactions with the electronic subsystem of ceramics. At the same time, irradiation with low-energy ions leads to large values of atomic displacements due to the large contribution of ionization losses as a result of interactions with nuclei. In this case, low energy irradiation leads to the formation of structural defects caused by the distortion and deformation of the crystal lattice, as well as subsequent swelling processes associated with the implantation and agglomeration of implanted ions. In the case of neutron irradiation, transmutational reactions are an important factor in radiation damage, leading to the accumulation of nuclear reaction products in the material, as well as residual radiation. At the same time, transmutation reactions, generally, lead to processes of material swelling and embrittlement, which negatively affect the properties and duration of the materials. Irradiation with heavy ions comparable to fission fragments of uranium nuclei, with energies of 150–250 MeV, in turn, is accompanied by both processes of change in electron density, as a result of the dominance of ionization losses on electronic shells, and processes associated with the formation of primary but knocked out atoms, in the maximum length of ion travel, when nuclear losses begin to prevail in energy losses.

The aim of this study is to evaluate the radiation resistance and deformation of the crystal structure of lithium-containing Li_2ZrO_3 ceramics depending on the fluence of irradiation with heavy Xe^{22+} ions with an energy of 230 MeV. The use of these ions will make it possible to simulate radiation damage arising from the operation of these materials in a nuclear reactor in contact with nuclear fuel during the formation of uranium fission fragments [27,28].

2. Experimental Part

Li_2ZrO_3 ceramics obtained by solid-phase synthesis with subsequent thermal annealing were chosen as the samples under study. The sample was prepared from a mixture of two powders of $LiClO_4 \cdot 3H_2O$ and ZrO_2 milled in a 1:1 ratio. The chemicals used were purchased from Sigma Aldrich (Saint Louis, MI, USA). The chemical purity of the selected reagents was 99.95%. Samples were ground in a PULVER-ISETTE 6 planetary mill (Fritsch Laboratory Instruments, Idar-Oberstein, Germany) in a tungsten carbide beaker. The volume ratio of grinding balls and reagents was 5:1, which is regulated by the installation certificate. Grinding was carried out at a grinding rate of 400 rpm for 1 hour, after which, the resulting milled powder was subjected to dispersion and further thermal annealing.

The samples were annealed in a muffle furnace at a temperature of 1100 °C for 5 h, followed by cooling for 24 h until reaching room temperature in the chamber.

Analysis of the synthesized sample phase composition showed that the synthesized samples are polycrystalline structures with a monoclinic phase with a spatial syngony C2/c(15) (see Figure 1a). According to the PDF-2 (2016) database, the lattice parameters

of Li_2ZrO_3 (PDF-01-070-8744) were a = 5.424 Å, b = 9.0263 Å, c = 5.4197 Å, β = 112.701°, V = 244.79 Å^3.
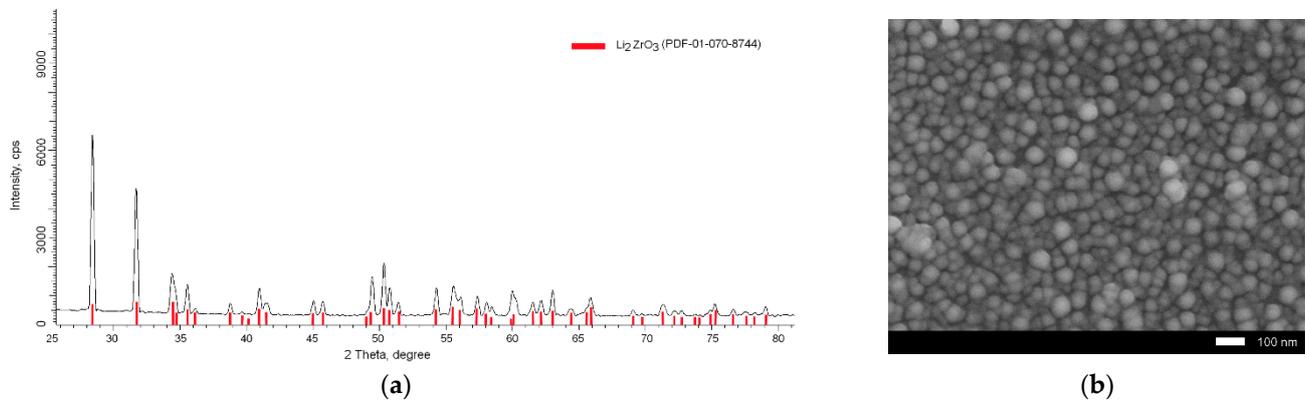
Figure 1. (**a**) X-ray diffraction pattern of the initial ceramic sample after sintering; (**b**) SEM - image of the initial sample surface after sintering and pressing.

Study of the morphological features of ceramics was carried out using the scanning electron microscopy method, implemented using a Jeol F7500 (Jeol, Tokyo, Japan). According to the obtained data of images of samples in the initial state, the morphology of ceramics is represented by spherical particles, the size of which is 90–110 nm, and the homogeneity of sizes is more than 90% (see Figure 1b).

The samples were irradiated on a DC-60 heavy ion accelerator (Institute of Nuclear Physics, Almaty, Kazakhstan). To simulate the processes of radiation damage and subsequent swelling and embrittlement as a result of the accumulation of point defects and implanted ions, beams of heavy Xe^{22+} ions with an energy of 230 MeV (1.75 MeV/nucleon) were used. The irradiation fluence was 10^{11}–10^{16} ion/cm^2, and the irradiation was carried out in vacuum at room temperature. In order to avoid the effect of heating the samples during irradiation, the samples were placed on a special water-cooled target holder that kept the temperature of the sample within 50–60 °C.

The simulation of radiation damage and the ion path length in the ceramic material was carried out using the SRIM Pro 2013 program code [29,30]. The Kinchin–Pease model [30] was used as a model; the density of ceramics was chosen according to the X-ray phase analysis data of 4.2 g/cm^3. The threshold displacement energies were taken from the literature data for similar studies [31]. According to the calculated data, the energy losses of incident Xe^{22+} ions with an energy of 230 MeV are $dE/dx_{electron}$ = 19750 keV/μm, $dE/dx_{nuclear}$ = 65.6 keV/μm. At the selected energies of incident ions, the main contribution to the defect formation processes is made by electron energy losses of ions over most of the trajectory of motion in the material. In the case where the ion is close to reaching the maximum penetration depth, a balance of energy losses occurs during the interaction of ions with electron shells and nuclei, which leads to the appearance of a maximum of displacements at a depth of 14.5–15.5 μm.

The calculations of the values of atomic displacements and the concentration of implanted ions were carried out using the method proposed by G.W. Egeland et al. in [32]. Calculations of the displacement per atom (dpa) depending on the penetration depth were carried out using the equation:

$$dpa = \left(\frac{10^8 \times \text{fluence}}{8.38 \times 10^{22}} \right) \times (\text{Vacancy.txt}), \tag{1}$$

Vacancy.txt—a calculation file taken from the results of simulation of the processes of radiation damage and the travel depth using the SRIM Pro 2013 program code.

The concentration of implanted ions as a result of irradiation was determined using Equation (2):

$$at.\%ion = \left(\frac{\text{fluence}}{8.38 \times 10^{22}} \right) \times (\text{range.txt}) \times 100, \tag{2}$$

Range.txt—a calculation file taken from the results of simulation of the processes of radiation damage and the travel depth using the SRIM Pro 2013 program code. The simulation results are shown in Figure 2.
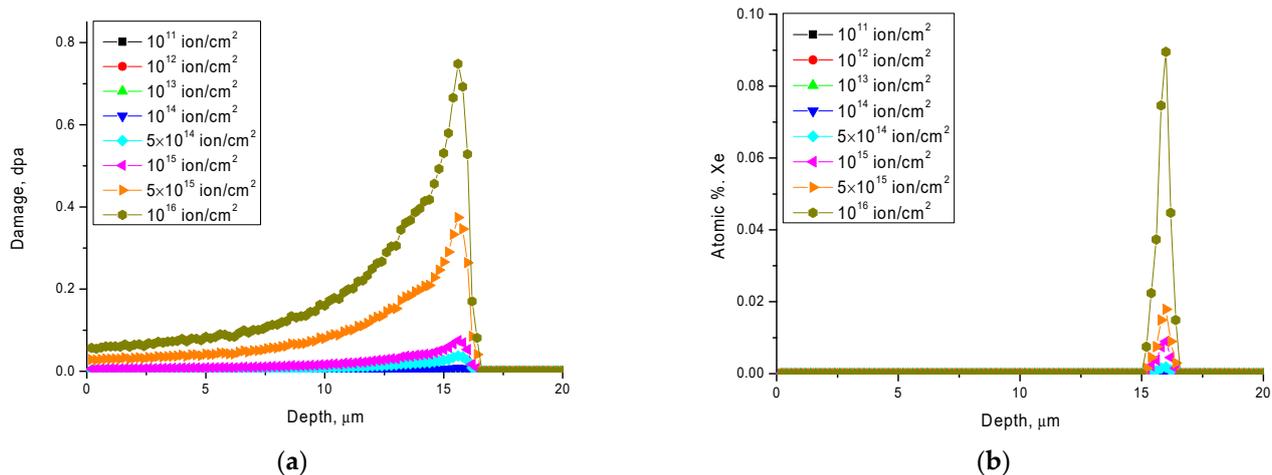
Figure 2. (**a**) Graph of displacements per atom versus radiation fluence; (**b**) graph of the implanted Xe^{22+} ion concentration versus irradiation fluence.

According to the simulation results obtained, the maximum displacement for the irradiation fluences of 10^{15}–10^{16} ions/cm^2 at the maximum ion penetration depth is from 0.1 to 0.7 dpa, whereas the concentration of implanted ions is no more than 0.02–0.09 at. %. Such displacement values are due to the fact that, for heavy ions, the main contribution to radiation damage is made by elastic interactions of incident ions with electron shells, as a result of which, electrons are knocked out, followed by a redistribution of the electron density along the trajectory of ions in the material.

The study of structural changes as a result of irradiation with heavy ions was carried out using the method of full-profile analysis of X-ray diffraction patterns obtained with a D8 Advance ECO (Bruker, Karlsruhe, Germany) powder X-ray diffractometer. Diffraction patterns were obtained in the Bragg–Brentano geometry, in the angular range of 2θ = 25–80°, with a step of 0.03°; a copper tube with a wavelength of Cu-kλ = 1.54 Å was used as an X-ray source. The X-ray diffractometer was calibrated using a standard technique for refining the parameters and broadening diffraction lines; Korundprobe A13-B77 (F-№16/10-2302) (Briker AXS, Karlsruhe, Germany) was used as a reference sample. The structural parameters were refined using the DiffracEVA v.4.2 (Bruker, Ettlingen, Germany) program code. Determination of the structural perfection degree (crystallinity degree) was carried out by comparative analysis of the diffraction maxima areas with areas characteristic of background radiation and disorder areas. Diffraction patterns were taken by selecting both filters and the accelerating voltage of the tube so that the maximum penetration depth of X-rays into the sample was no more than 15–20 μm. The purpose of the selection of such conditions was to obtain X-ray diffraction patterns from the irradiated part of the samples to determine the change in the structural properties of the irradiated ceramic layer.

Determination of the strength properties of ceramics, as well as the determination of radiation resistance to degradation and softening, was carried out by measuring micro-hardness value of the ceramics. The microhardness was determined by the indentation method, where a Vickers diamond pyramid was used as an indenter and the load on the indenter was 1000 N. This method allows for the determination of the hardness value from

indenter imprint, and value of swelling degree and hardness decrease is determined by difference in hardness readings for samples before and after irradiation.

3. Results and Discussion

Figure 3 shows the results of changes in the X-ray diffraction patterns of the samples under study depending on the irradiation fluence. An analysis of the data obtained revealed the absence of any new diffraction reflections for irradiated samples, which indicates the absence of phase polymorphic transformations caused by irradiation or the formation of impurity phases as a result of strong structural disordering.
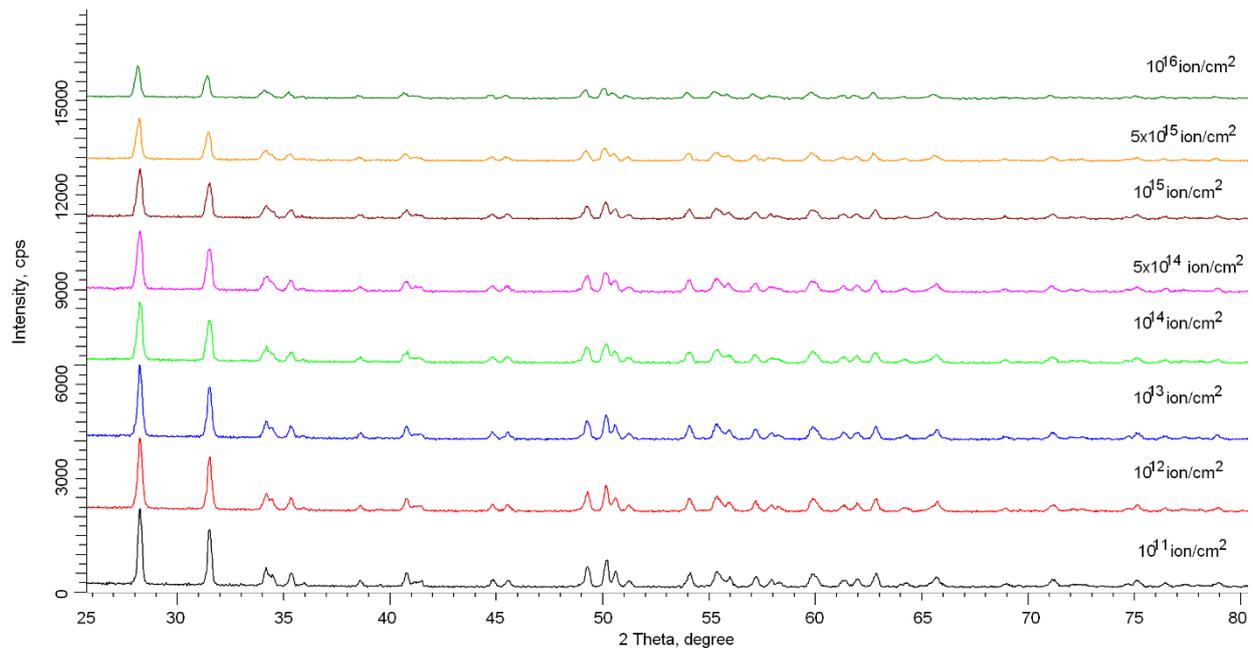
Figure 3. X-ray diffraction patterns of the studied ceramics depending on irradiation fluence.

The main changes in diffraction patterns depending on the irradiation fluence observed in the figure are associated with a change in the shape, intensity and position of diffraction lines, which is characteristic of structural changes associated with the deformation and distortions of the crystal structure as a result of external influences. At the same time, the greatest changes are observed for samples irradiated with fluences above 5×10^{14} ion/cm^2, for which, not only a decrease in their reflection intensity is observed, but also their shift to the region of small angles, which indicates a deformation and distortions of interplanar distances. Applying the Rietveld method and the Williamson–Hall construction to assess the change in the angular value of FWHM, which characterizes the deformation and size effects that affect the change in diffraction patterns, the contributions of the deformation and distortion of the crystal lattice were determined. The results are shown in Figure 4. According to the obtained angular dependences, in the case of irradiation fluences above 10^{14} ion/cm^2, a change in the slope of FWHM curves is observed, which indicates an increase in the distortion and deformation degree of the crystal lattice. At the same time, comparing coefficients in equations describing these dependences, reflecting the deformation value, it was found that, at irradiation fluences above 10^{15} ions/cm^2, the deformation value is an order higher than that of ceramics in the initial state.
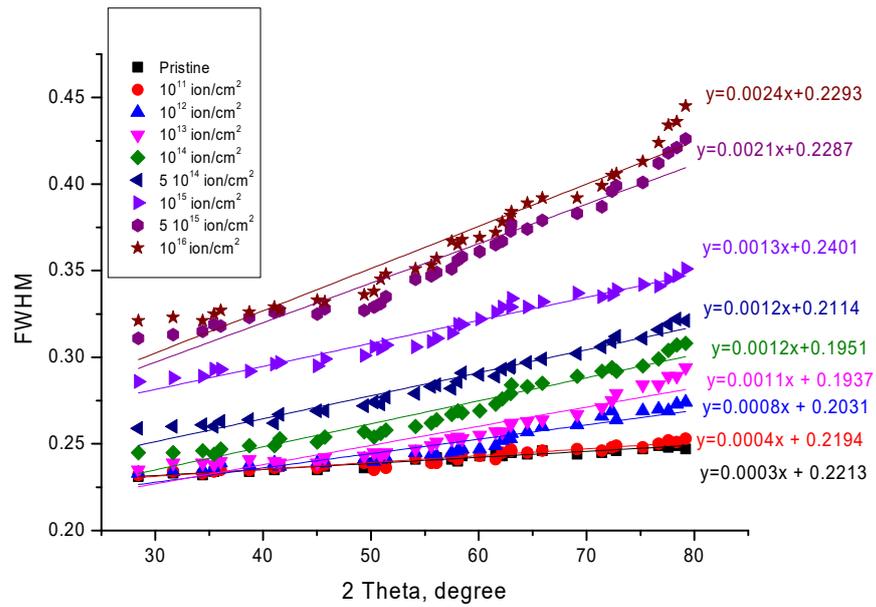
Figure 4. Angular dependences of changes in the FWHM values of the studied ceramics.

Based on the data obtained, the crystal lattice parameters were calculated, which reflect its change as a result of external influences associated with the crystal structure deformation and its swelling. Table 1 shows the data of changes in the structural parameters determined for the irradiated samples depending on the irradiation fluence. The parameters were refined using the Nelson–Taylor equations.

Table 1. Data on changes in the crystal lattice parameters depending on the radiation fluence.

Sample	Fluence, ion/cm^2								
	Pristine	10^{11}	10^{12}	10^{13}	10^{14}	5×10^{14}	10^{15}	5×10^{15}	10^{16}
Lattice parameter, Å	a = 5.3868	a = 5.3889,	a = 5.3911,	a = 5.3953,	a = 5.3997,	a = 5.4083,	a = 5.4169,	a = 5.4371,	a = 5.4641,
	b = 8.9856	b = 8.9892,	b = 8.9928,	b = 8.9999,	b = 9.0108,	b = 9.0443,	b = 9.0588,	b = 9.0961,	b = 9.1532,
	c = 5.4038	c = 5.4059,	c = 5.4081,	c = 5.4124,	c = 5.4189,	c = 5.4327,	c = 5.4457,	c = 5.4767,	c = 5.5241
	β = 112.06	β = 112.63	β = 112.24°	β = 112.17°	β = 112.33°	β = 112.66°	β = 112.77°	β = 113.06°	β = 113.45°
Lattice volume, Å^3	241.93	242.63	242.84	243.27	243.89	245.23	246.46	249.21	253.65
Density, g/cm^3	4.202	4.191	4.187	4.179	4.169	4.145	4.125	4.079	4.008

Based on the obtained lattice volume change data, the ceramic density was calculated according to the standard density estimation technique using the radiographic method. It is prudent to mention that these calculations are in good agreement with the density determination results obtained using the standard Archimedes method. As can be seen from the data presented, an increase in the crystal lattice volume as a result of swelling under the action of irradiation leads to a decrease in porosity, which, at maximum irradiation fluences of 10^{15}–10^{16} ions/cm^2, was more than 3–4%.

As can be seen from the data presented, the main changes in crystal lattice parameters are associated with an increase in its dimensions depending on irradiation fluence, as well as an increase in the lattice volume, which indicates crystal lattice swelling. Based on the obtained data on changes in the crystal lattice parameters, the degree of deformation and distortion of the crystal lattice axes was estimated depending on the irradiation fluence. The results are shown in Figure 5.
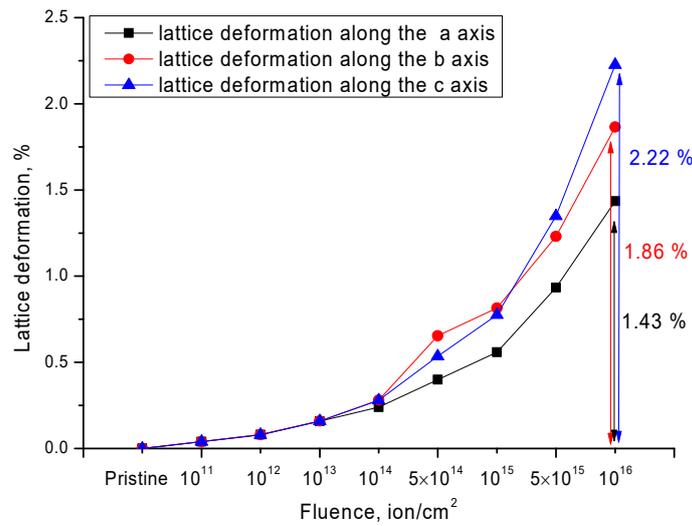
Figure 5. Dynamics of the crystal lattice deformation depending on irradiation fluence.

At irradiation fluences of 10^{11}–10^{14} ion/cm^2, changes in the crystal lattice parameters along all axes are equally probable, which indicates that the distortions and deformations arising as a result of irradiation are isotropic. However, the accumulation of radiation damage and the concentration of implanted Xe^{22+} ions leads to an anisotropy of crystal lattice distortions, as evidenced by different deformation values. According to the data obtained, the crystal lattice is most resistant to deformation along the *a* crystallographic axis, whereas the lattice deformations along the *b* and *c* axes are more pronounced. Thus, it can be concluded that irradiation at high fluences leads to an anisotropic distortion of the crystal structure due to the formation of defect regions in the structure, as well as the partial replacement of atoms in the crystal lattice sites by implanted ions.

The crystal lattice swelling was estimated by calculating the difference between the volume of the crystal lattice of irradiated (V) and initial (V_0) samples and using Equation (3). The results are shown in Figure 6.

$$\text{Swelling} = \frac{V - V_0}{V_0} \times 100\% \tag{3}$$
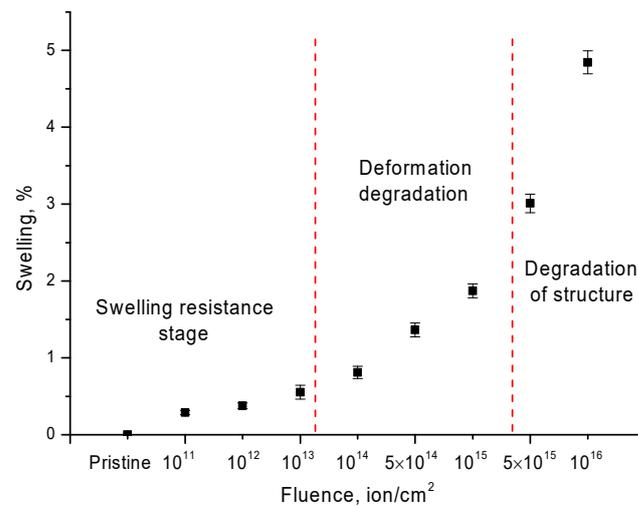
Figure 6. Dynamics of changes in the crystal lattice swelling value.

The general view of the dynamics of changes in the crystal lattice swelling value can be divided into three stages that are characteristic of various fluences. The first stage is typical for irradiation fluences of 10^{11}–10^{13} ion/cm^2 and is characterized by small changes

in the swelling value of less than 0.5%, which indicates that the stability of the crystal lattice of ceramics to swelling and deformation remains unchanged. As is known, for these irradiation fluences, the formation of point defects isolated from each other is most likely, since the trajectories of ions in the material do not have a high probability of overlap. At the same time, all defects formed along the trajectory of ion motion in the material have an isolated character, which leads to their rapid annihilation and a low probability of the formation of defect complexes or their accumulations. A slight increase in the crystal lattice deformation degree, leading to its swelling, is due to deformation and distorting processes arising from the interaction of incident ions with the crystal lattice and the knocking out of atoms from the lattice sites.

The second stage is typical for irradiation fluences of 10^{14}–10^{15} ion/cm^2. At this stage, there is a linear increase in the swelling value associated with an increase in crystal lattice distortions and its deformation as a result of the radiation damage accumulation. At the same time, an assessment of the probability of overlapping the trajectories of incident ions in the structure of materials for these fluences showed that the amount of overlap is from 10 to 100, which leads to the formation of high-defect areas and agglomeration of point defects. An increase in the overlapping regions of ion trajectories in the material leads to the fact that some of the formed point defects cease to be isolated from each other and begin to interact with each other, which leads to the formation of two-dimensional or cluster defects. At the same time, there is a possibility that several ions can get into the same place, which can lead to an increase in the degree of disordering of the structure in the previously damaged area. It is also worth noting that, unlike metals, for which the effect of self-healing and relaxation of changes in electron density due to high mobility is possible, in dielectric ceramics, this effect is difficult due to the dielectric nature of the material. As a result, changes in the electron density caused by irradiation can persist for a sufficiently long time, which leads to the appearance of metastable states in the structure, which are more susceptible to deformation as a result of external influences. In turn, an increase in these regions in the structure, as a result of an increase in the irradiation fluence, leads to an increase in crystal lattice distortions and a decrease in the resistance of ceramics to irradiation.

The third stage is typical for irradiation fluences of 5×10^{15}–10^{16} ion/cm^2, for which, according to the calculated data, the concentration of implanted ions into the structure is more than 0.05 at.%, and the dpa value varies from 0.4 to 0.7 dpa. At the same time, an increase in the irradiation fluence leads to a sharp increase in the crystal lattice swelling, accompanied by strong distortions of the crystal lattice and its deformation. This crystal structure behavior is due to the radiation damage accumulation associated with strong crystal structure disordering and the implantation of ions into the sites and interstices of the crystal lattice. The accumulation of implanted ions in the structure can lead to the filling of their pores and voids with subsequent agglomeration and the formation of gas inclusions. The presence of such inclusions in the structure of ceramics leads to their degradation and a decrease in their strength properties.

Figure 7 shows the results of changes in the microhardness indices and the degree of softening of ceramics depending on the irradiation fluence. The softening degree (SD) was estimated based on data of changes in hardness in the initial (H_0) and irradiated (H) state (4):

$$\text{SD} = \frac{H_0 - H}{H_0} \times 100\% \tag{4}$$
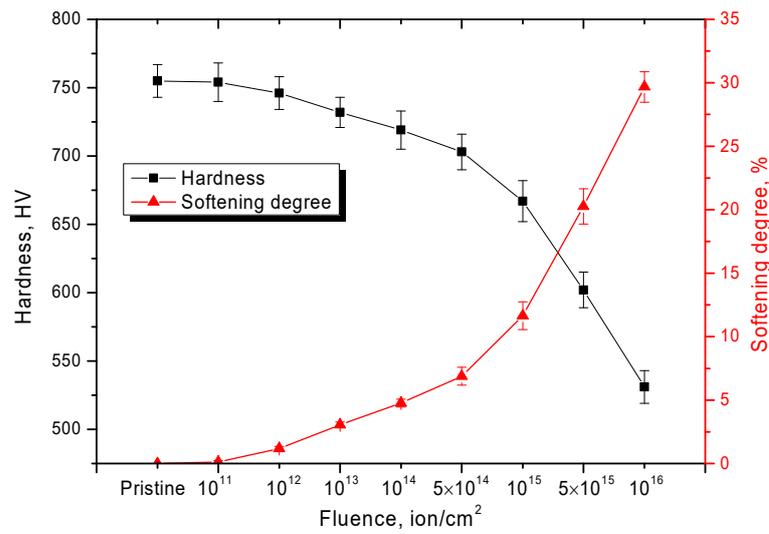
Figure 7. Data on changes in strength properties depending on irradiation fluence.

The general view of changes in the hardness and softening degree of the near-surface layer of ceramics, depending on the fluence, agrees with the results of changes in the structural properties and the crystal structure swelling degree. At low irradiation fluences, the change in microhardness is less than 2–5%, which indicates a fairly high disordering and degradation resistance degree. An increase in the irradiation fluence above 10^{14} ion/cm^2 leads to a sharp increase in the softening degree, which indicates an accelerated destruction of the surface layer as a result of a strong deformation of the crystal structure and radiation damage accumulation.

Figure 8 shows the results of changes in the morphological features of the surface layer of ceramics after irradiation with maximum fluences of 5×10^{15}–10^{16} ion/cm^2.
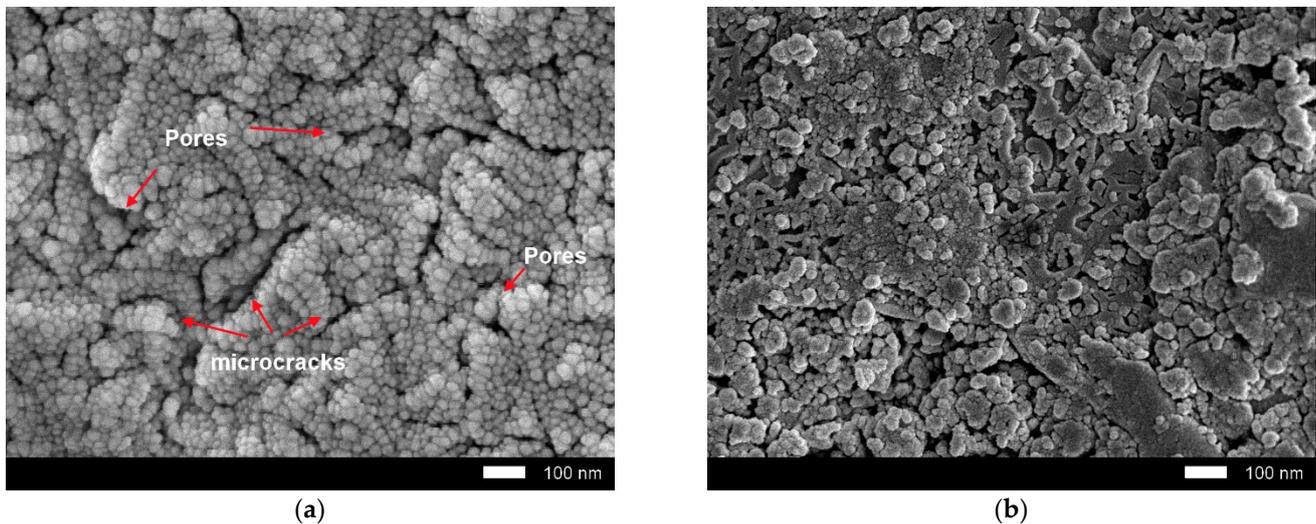
Figure 8. SEM images of the surface layer of ceramics after irradiation with fluences: (**a**) 5×10^{15} ion/cm^2; (**b**) 10^{16} ion/cm^2.

As can be seen from the data presented, structural distortions and the swelling of ceramics as a result of radiation damage lead to the formation of microcracks and pores. The result is a decrease in both the strength and radiation damage resistance of ceramics. At the same time, an increase in the irradiation fluence up to ion/cm^2 leads to the embrittlement processes of the near-surface layer and partial destruction of ceramics.

4. Conclusion

The aim of this work is to study the radiation damage kinetics and the degree of resistance to the radiation embrittlement and swelling of Li_2ZrO_3 ceramics obtained by solid-phase synthesis. Scanning electron microscopy, X-ray phase analysis and a determination of the microhardness were used as research methods. During the studies carried out, dependences of the change in the structural properties and the degree of their degradation as a result of the radiation damage accumulation on the irradiation fluence and the concentration of implanted ions were established. It was found that the greatest degradation degree of ceramics is observed at irradiation fluences of 10^{15}–10^{16} ion/cm^2, which corresponds to a value of 0.4–0.7 dpa. At such displacement values, a strong crystal structure disordering is observed, caused by crystal lattice distortions and its swelling.

Institutional Review Board Statement: Not applicable.

Informed Consent Statement: Informed consent was obtained from all individual participants included in the study.

Data Availability Statement: Not applicable.

Conflicts of Interest: The authors declare no conflict of interest.

References

1. Liu, L.; Deng, J.; Zhang, D.; Gu, H. Review of the experimental research on the thermal-hydraulic characteristics in the pebble bed nuclear reactor core and fusion breeder blankets. *Int. J. Energy Res.* **2021**, *45*, 11352–11383. [CrossRef]
2. Noda, T. Advanced SiC-SiC Composites for Nuclear Application. In *Handbook of Advanced Ceramics and Composites: Defense, Security, Aerospace and Energy Applications*; Springer Nature Switzerland AG: Cham, Switzerland, 2020; pp. 641–666.
3. Maemunah, I.R.; Su'Ud, Z.; Waris, A.; Irwanto, D. Study on fusion blanket with ceramic solid as tritium breeding material. *J. Phys. Conf. Ser.* **2021**, *2072*, 012004. [CrossRef]
4. Samolyuk, G.; Edmondson, P. First principles study of the stability and thermal conductivity of novel Li-Be hybrid ceramics. *Acta Mater.* **2021**, *215*, 117052. [CrossRef]
5. Kim, J.-I.; Park, Y.-H.; Ahn, M.-Y.; Kishimoto, H.; Lee, Y.; Cho, S. Effects of sintering conditions on the microstructure of Li2TiO3 tritium breeding materials. *Fusion Eng. Des.* **2020**, *156*, 111727. [CrossRef]
6. Batyrbekov, E.; Khasenov, M.; Gordienko, Y.; Samarkhanov, K.; Ponkratov, Y. Optical radiation from the sputtered species under gas excitation by the products of the $^6Li(n,\alpha)^3H$ nuclear reaction. *J. Lumin.* **2020**, *220*, 116973. [CrossRef]
7. Gu, S.; Qi, Q.; Zhang, Y.; Ji, B.; Zhou, H.; Luo, G.-N. Mechanical strength stability of tritium breeding materials under high temperature deuterium conditions. *Ceram. Int.* **2020**, *46*, 1195–1202. [CrossRef]
8. Sahoo, D.R.; Chaudhuri, P.; Swaminathan, N. A molecular dynamics study of displacement cascades and radiation induced amorphization in Li_2TiO_3. *Comput. Mater. Sci.* **2021**, *200*, 110783. [CrossRef]
9. Ba, J.; Zeng, R.; Yan, X.; Li, R.; Wu, W.; Li, F.; Xiang, X.; Meng, D.; Tang, T. Long-term helium bubble evolution in sequential He$^+$ and H$^+$ irradiated Li_4SiO_4. *Ceram. Int.* **2021**, *47*, 32310–32317. [CrossRef]
10. Shlimas, D.I.; Zdorovets, M.V.; Kozlovskiy, A.L. Synthesis and resistance to helium swelling of Li_2TiO_3 ceramics. *J. Mater. Sci. Mater. Electr.* **2020**, *31*, 12903–12912. [CrossRef]
11. Blynskiy, P.; Chikhray, Y.; Kulsartov, T.; Gabdullin, M.; Zaurbekova, Z.; Kizane, G.; Kenzhin, Y.; Tolenova, A.; Nesterov, E.; Shaimerdenov, A. Experiments on tritium generation and yield from lithium ceramics during neutron irradiation. *Int. J. Hydrog. Energy* **2021**, *46*, 9186–9192. [CrossRef]
12. Kulsartov, T.; Kenzhina, I.; Chikhray, Y.; Zaurbekova, Z.; Kenzhin, Y.; Aitkulov, M.; Gizatullin, S.; Dyussambayev, D. Determination of the activation energy of tritium diffusion in ceramic breeders by reactor power variation. *Fusion Eng. Des.* **2021**, *172*, 112783. [CrossRef]
13. Zinkle, S. Effect of H and He irradiation on cavity formation and blistering in ceramics. *Nucl. Instrum. Methods Phys. Res. Sect. B Beam Interact. Mater. Atoms* **2012**, *286*, 4–19. [CrossRef]
14. Zinkle, S. Effect of irradiation spectrum on the microstructural evolution in ceramic insulators. *J. Nucl. Mater.* **1995**, *219*, 113–127. [CrossRef]

15. Van der Laan, J.; Fedorov, A.; van Til, S.; Reimann, J. Ceramic Breeder Materials. *Compr. Nucl. Mater.* **2012**, *1*, 463–510. [CrossRef]
16. Ji, B.; Gu, S.; Qi, Q.; Li, X.-C.; Zhang, Y.; Zhou, H.; Luo, G.-N. Annihilation kinetics of irradiation defects in promising tritium breeding pebbles. *Nucl. Mater. Energy* **2021**, *27*, 101015. [CrossRef]
17. Rex, K.A.; Iyngaran, P.; Kuganathan, N.; Chroneos, A. Defect Properties and Lithium Incorporation in Li$_2$ZrO$_3$. *Energies* **2021**, *14*, 3963. [CrossRef]
18. Leys, J.M.; Zarins, A.; Cipa, J.; Baumane, L.; Kizane, G.; Knitter, R. Radiation-induced effects in neutron-and electron-irradiated lithium silicate ceramic breeder pebbles. *J. Nucl. Mater.* **2020**, *540*, 152347. [CrossRef]
19. Nishikawa, Y.; Oyaidzu, M.; Yoshikawa, A.; Munakata, K.; Okada, M.; Nishikawa, M.; Okuno, K. Correlation between tritium release and thermal annealing of irradiation damage in neutron-irradiated Li$_2$SiO$_3$. *J. Nucl. Mater.* **2007**, *367*, 1371–1376. [CrossRef]
20. Gu, S.; Ji, B.; Qi, Q.; Wang, J.; Zhou, H.; Zhang, Y.; Luo, G.-N. The effects of irradiation and high temperature on chemical states in Li$_2$TiO$_3$. *Int. J. Hydrog. Energy* **2019**, *44*, 32151–32157. [CrossRef]
21. Mirzayev, M.N. Simultaneous measurements of heat flow rate and thermal properties of nano boron trioxide under neutron irradiation at the low and high temperature. *Vacuum* **2020**, *173*, 109162. [CrossRef]
22. Mirzayev, M.N.; Popov, E.; Demir, E.; Abdurakhimov, B.A.; Mirzayeva, D.M.; Sukratov, V.A.; Kristavchuk, O. Thermophysical behavior of boron nitride and boron trioxide ceramics compounds with high energy electron fluence and swift heavy ion irradiated. *J. Alloys Compd.* **2020**, *834*, 155119. [CrossRef]
23. Tashmetov, M.; Abdurakhimov, B.; Mirzayev, M.N.; Thang, T.X. The effect of electron beam on nanocrystallites size, strain and structural parameters of the silicon carbide nanopowder. *Int. J. Mod. Phys. B* **2019**, *33*, 1950223. [CrossRef]
24. Pomaro, B. A Review on Radiation Damage in Concrete for Nuclear Facilities: From Experiments to Modeling. *Model. Simul. Eng.* **2016**, *2016*, 1–10. [CrossRef]
25. Demir, E.; Mirzayev, M.; Popov, E.; Horodek, P.; Genov, I.; Siemek, K.; Mirzayeva, D.; Turchenko, V.; Bulavin, M.; Beskrovnyi, A.; et al. Effects of high-energetic ^{3}He$^+$ ion irradiation on tungsten-based composites. *Vacuum* **2021**, *184*, 109934. [CrossRef]
26. Buzi, L.; Yeh, M.; Yeh, Y.-W.; Donaldson, O.; Patino, M.; Trelewicz, J.; Yao, N.; Doerner, R.; Koel, B. Deuterium and helium ion irradiation of nanograined tungsten and tungsten–titanium alloys. *Nucl. Mater. Energy* **2019**, *21*, 100713. [CrossRef]
27. Budzyński, P.; Kamiński, M.; Surowiec, Z.; Wiertel, M.; Skuratov, V.; Korneeva, E. Effects of xenon-ion irradiation on the tribological properties and crystal structure of titanium and its alloy Ti6Al4V. *Tribol. Int.* **2021**, *156*, 106854. [CrossRef]
28. Ivanov, I.A.; Alin, M.; Koloberdin, M.V.; Sapar, A.; Kurakhmedov, A.E.; Kozlovskiy, A.L.; Zdorovets, M.V.; Uglov, V.V. Effect of irradiation with heavy Xe^{22+} ions with energies of 165–230 MeV on change in optical characteristics of ZrO$_2$ ceramic. *Optical Materials* **2021**, *120*, 111479. [CrossRef]
29. Agarwal, S.; Lin, Y.; Li, C.; Stoller, R.E.; Zinkle, S.J. On the use of SRIM for calculating vacancy production: Quick calculation and full-cascade options. *Nucl. Instrum. Methods Phys. Res. Sect. B Beam Interact. Mater. Atoms* **2021**, *503*, 11–29. [CrossRef]
30. Ziegler, J.F.; Ziegler, M.D.; Biersack, J.P. SRIM–The stopping and range of ions in matter (2010). *Nucl. Instrum. Methods Phys. Res. Sect. B Beam Interact. Mater. Atoms* **2010**, *268*, 1818–1823. [CrossRef]
31. Sickafus, K.E.; Hartmann, T.; Yasuda, K.; Valdez, J.A.; Chodak, P., III; Nastasi, M.; Verrall, R.A. Radiation damage effects in zirconia. *J. Nuclear Mater.* **1999**, *274*, 66–77. [CrossRef]
32. Egeland, G.; Valdez, J.; Maloy, S.; McClellan, K.; Sickafus, K.; Bond, G. Heavy-ion irradiation defect accumulation in ZrN characterized by TEM, GIXRD, nanoindentation, and helium desorption. *J. Nucl. Mater.* **2013**, *435*, 77–87. [CrossRef]